Reference: *Biol. Bull.* **214:** 315–318. (June 2008)

Hydrodynamic Context for Considering Turbulence Impacts on External Fertilization

BRIAN GAYLORD

Bodega Marine Laboratory and Section of Evolution and Ecology, University of California at Davis, Bodega Bay, California 94923

Wave-swept shores in the marine environment are characterized by turbulent water motion. This turbulence influences external fertilization in benthic organisms by diluting gametes and producing hydrodynamic shear that is believed to have the capacity to disrupt egg-sperm interaction. However, although turbulence levels associated with decreases in fertilization due to this latter process (shear) have been identified in the laboratory, estimates of the intensities of turbulence in intertidal habitats have been based primarily on scaling arguments of limited precision and unknown accuracy. In the present study, values of energy dissipation rate (a standard measure of the strength of turbulence) were determined for three locations in the surf zone of a rocky shore. These measurements suggest a potential correspondence between threshold levels of turbulence that impair the ability of sperm to fertilize eggs, and actual intensities of turbulence arising in nature.

Fertilization success in broadcast spawners is thought to be influenced by fluid turbulence. When the intensity of turbulence is mild or moderate, the increased mixing that accompanies it may facilitate gamete contact and elevate fertilization rates (1). Under conditions of extreme turbulence, however, gametes are rapidly diluted and strong viscous shear associated with the smallest scales of turbulent motion may disrupt critical interactions between egg and sperm (2–4). Such extreme turbulence is believed to arise routinely in the "white water" of intertidal habitats subjected to actively breaking waves.

Intensities of turbulence are typically quantified in terms of the energy dissipation rate (ε), an index of how fast the kinetic energy of a flow is transferred from larger scales of motion to smaller ones, and in the limit, converted to heat. Laboratory work with gametes held in confined chambers (thus eliminating dilution effects) indicates that energy dissipation rates from 0.1–0.5 W/kg improve fertilization success, while larger values of ε disrupt it (2–4). Theoretical scaling calculations have then been used to connect these energy dissipation rates to field conditions, focusing on intertidal habitats where turbulence intensities are highest (5).

Unfortunately, although such scaling analyses are based on appropriately assumed equivalence between the amount of wave energy entering a surf zone and the energy dissipated within it, they lead to only weakly bounded estimates. This limitation arises for the following reasons. First, even though wave energies incident on a shore can be quantified (5), a portion of this energy is reflected and either does not enter the surf zone or does not remain there. This fraction can vary from less than 0.1 to almost 1.0. Second, calculations of ε require an estimation of the spatial "volume" of intertidal habitat in which the arriving energy is dissipated. Denny *et al.* (5) provide useful approximations for idealized coastal geometries, but because volume is computed as the cube of a given linear dimension, even moderate adjustment to such dimensions can appreciably change the calculation. Third, two commonly invoked models for surf-zone energy dissipation rate (5, 6) predict values that vary in contrasting ways with wave height (*i.e.,* as either H^3 or $H^{1/2}$, where H is wave height). The power-of-six difference in exponent introduces substantial additional ambiguity. Together, these summed sources of error create 2 to 3 orders of magnitude of uncertainty, thereby obscuring the ecological and evolutionary roles of turbulence in marine reproduction.

In the present study, such uncertainty was confronted through direct quantification of turbulence in the field. High-frequency, 1000-Hz velocity data were collected at three locations along a 500-m stretch of rocky shore at

Received 19 November 2007; accepted 13 February 2008.
* To whom correspondence should be addressed. E-mail: bpgaylord@ucdavis.edu

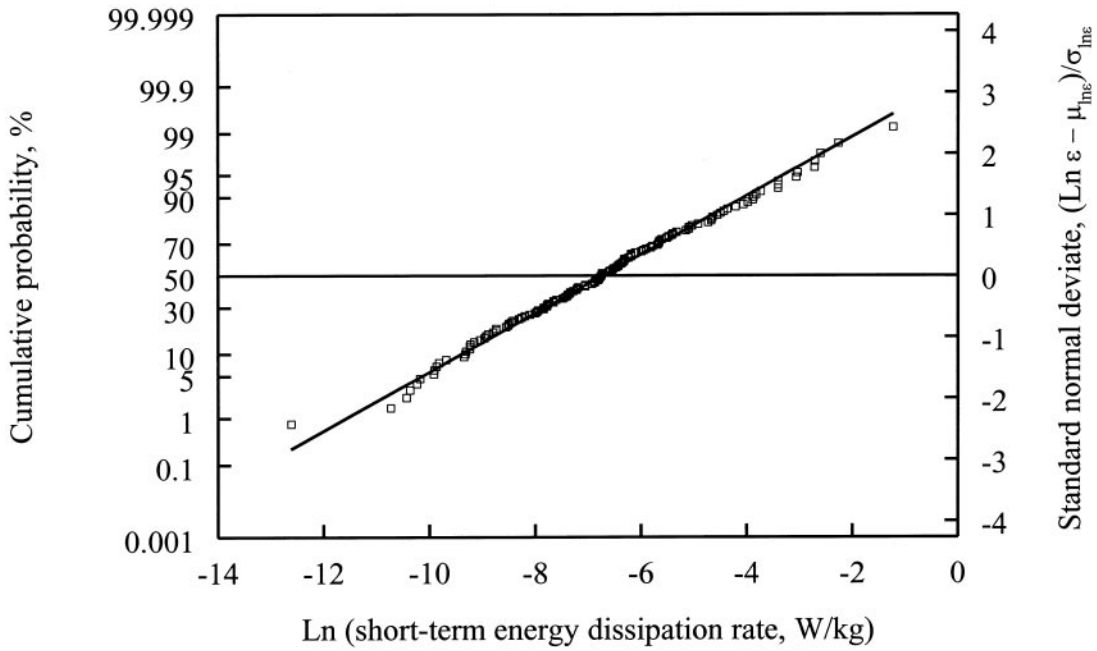

Figure 1. Collections of short-term energy dissipation rates (ε) plot as a straight line on a probability scale when ln-transformed, indicating a lognormal character. Individual dissipation rate estimates are based on 0.128-s, 1000-Hz velocity segments, analyzed following the methods of George *et al.* (10). Each segment was evaluated for adherence to Taylor's hypothesis (9) by requiring that $U > 5u_{\text{rms}}$, $U > 5\Delta U$, and $U > 5V$ or $5W$, where u_{rms} was the root-mean-square fluctuation in velocity about U, the mean horizontal velocity, ΔU was the maximum change in U during the segment, V was the mean velocity perpendicular to U, and W was the mean vertical velocity, assumed to be always small relative to U or V due to the flow probe's proximity to the substratum. For segments meeting these criteria, a frequency power spectrum was computed and converted to a wavenumber spectrum by means of Eq. 2. A line of $-5/3$ slope was fit to the log-transform of the first 32 spectral estimates, which corresponded to the low wavenumber end of the inertial subrange and covered frequencies ranging from approximately 8–250 Hz. Higher frequencies were eliminated from the regression because earlier low-pass filtering had already removed the upper end of the spectrum, and because the spatial limit of resolution of the flow probe was ~0.01 m, which yielded a maximum detectable turbulent frequency of approximately 300 Hz ($f \sim U/l \sim 3/0.01$ for typical mean flows in the field). The 8-Hz lower limit was dictated by the need to exclude from the regression low-frequency components of flow associated with residual features of the overall wave motion ($f \sim U/l$, with $U \sim 2H$ and $l \sim 0.25H$, where H is local wave height; [15]). The intercept, b, of the $-5/3$ slope fitted line was then used in conjunction with Eq. 1 to calculate the energy dissipation rate for each 0.128-s segment as $\varepsilon = [(55/27)(10^b)]^{3/2}$. Data shown encompass all velocity segments recorded under waves of 0.85–0.9 m intertidal height, at field location 1.

Hopkins Marine Station (Pacific Grove, California), using drag-sphere flow probes (7, 8). These instruments recorded fluid velocities at an elevation 2 cm above the substratum, at the height where many macroinvertebrates release their gametes, on multiple dates spanning several tidal cycles between 30 January 1995 and 1 August 1996. Properties of the well-known "turbulent cascade" (a process reflecting the stepwise transfer of kinetic energy from large to increasingly small length scales) were then employed to extract energy dissipation rates from the velocity records. Across an intermediate range of scales where flow structures (eddies) interact with minimal viscous loss (*i.e.,* across the inertial subrange; [9]), velocity fluctuations aligned with the mean flow follow the relationship

$$E(\kappa) = \frac{27}{55}\,\varepsilon^{2/3}\,\kappa^{-5/3} \tag{1}$$

This expression quantifies the amount of energy contained in eddies of a given spatial dimension, l (represented by a wavenumber, $\kappa = 2\pi/l$), in terms of $E(\kappa)$, the power spectrum of velocity in the so-called wavenumber domain. If there is also a strong mean velocity, U, the wavenumber spectrum can be replaced with a standard frequency spectrum, which is more readily measured. This conversion assumes that a stationary sensor encounters an eddy of spatial extent l for the duration $\tau = l/U$ (a relationship called Taylor's hypothesis; [9]) which in turn leads to the equalities

$$\kappa = \frac{2\pi f}{U} \qquad E(\kappa) = \frac{U}{2\pi} E(f) \tag{2}$$

where $f\,(=1/\tau)$ is frequency and $E(f)$ is the frequency power spectrum of the velocity fluctuations (10). Conveniently, when the logarithm of $E(\kappa)$ is plotted *versus* the logarithm of κ, the y-intercept enables calculation of the short-term energy dissipation rate associated with the underlying velocity record (Fig. 1). These short-term dissipation rates tend to follow a lognormal cumulative probability distribution (11), which means that longer-term average dissipation rates, $<\varepsilon>$, are given by

$$<\varepsilon> = \exp\left(\mu_{\ln\varepsilon} + \frac{{\sigma_{\ln\varepsilon}}^2}{2}\right) \tag{3}$$

where ${\sigma_{\ln\varepsilon}}^2$ is the variance of the natural logarithm of the short-term ε values (defining how intermittent the turbulence is), and $\mu_{\ln\varepsilon}$ is the mean of the normally distributed $\ln(\varepsilon)$ values.

Results of the present study confirmed that short-term energy dissipation rates in the surf zone routinely followed a lognormal distribution (Fig. 1). Values within this distribution ranged from less than 10^{-6} to greater than 10 W/kg, a breadth unsurprising for highly variable flows typical of intertidal habitats. The distributions of short-term dissipation rates also exhibited exceptional intermittency (${\sigma_{\ln\varepsilon}}^2$ from 2–14), which led to long-term mean energy dissipation rates as large as 1 W/kg (Fig. 2). These long-term mean dissipation rates exceeded by over an order of magnitude the largest turbulence levels recorded under breaking waves on gently sloping sandy beaches (0.05 W/kg; [10]). Such larger values are consistent with the observation that waves break with much greater violence on steep rocky shores. Results of Figure 2 also suggest an exponential relationship between energy dissipation rates and intertidal wave height across the modest wave heights (*i.e.,* non-storm conditions) encountered during the present study.

The measurements presented above represent a first attempt to determine turbulence levels on rocky shores. Although the data are nominally physical, their greatest utility arises in the context of the organisms that live in such habitats. Previous laboratory work with *Strongylocentrotus purpuratus*, the purple sea urchin, suggests that viscous shear associated with strong turbulence can dramatically reduce fertilization success even in the absence of gamete dilution (2, 3). Such declines in fertilization began in the prior studies at turbulence levels comparable to the largest of the mean energy dissipation rates determined here (~1 W/kg; Fig. 3). The earlier work also showed fertilization success plummeting 90% as turbulence levels reached 10 W/kg, near the largest short-term values recorded over durations of ~0.1 s (Fig. 1). Such correspondence between the "active" part of the curve in Figure 3 and the short- and

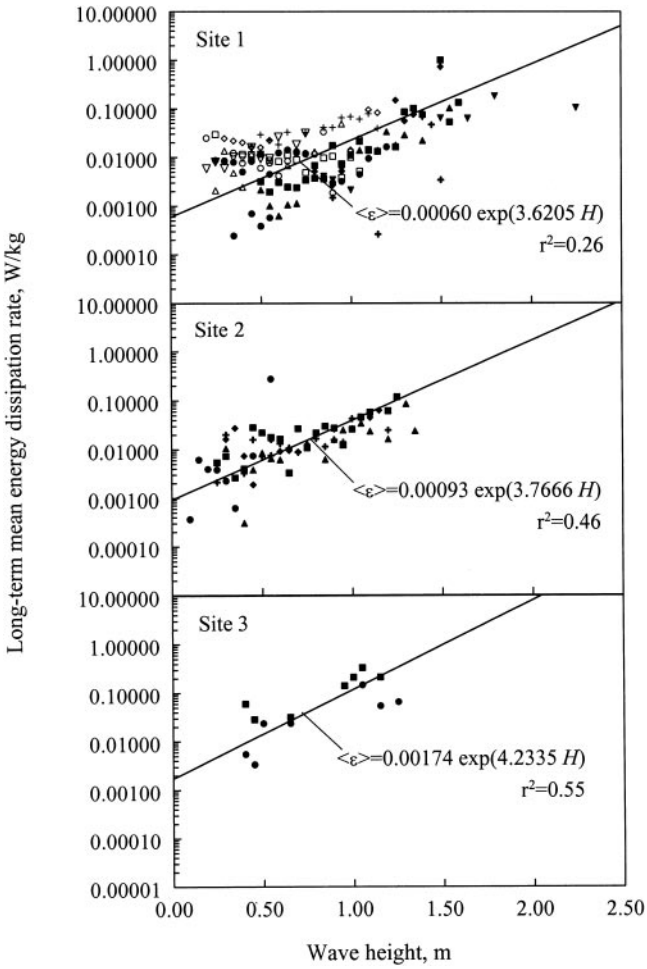

Figure 2. Long-term average energy dissipation rates, $<\varepsilon>$, for three field locations at Hopkins Marine Station, computed using Eq. 3 from values of $\mu_{\ln\varepsilon}$ and ${\sigma_{\ln\varepsilon}}^2$ determined from the slopes $(= 1/\sigma_{\ln\varepsilon})$ and intercepts $(= -\mu_{\ln\varepsilon}/\sigma_{\ln\varepsilon})$ of lines like those of Fig. 1. Note that in each panel, Model II regression lines on semilog axes suggest an exponential relationsip between average energy dissipation rate and intertidal wave height, H. Different symbols indicate distinct recording dates over the duration of the study.

long-term dissipation rates quantified here suggests that attributes of the time scales of gamete-turbulence interaction in the field could be critical. For instance, bursts of strong shear could constrain peak rates of fertilization if they disrupted egg-sperm interactions during brief periods of high gamete concentration prior to dilution (*e.g.,* immediately following spawning in dense aggregations of animals). Although many *S. purpuratus* individuals live in deeper waters where turbulence is weaker, the importance of this species as a model organism for studies of fertilization and early development also points to the possibility that additional taxa (including purely intertidal ones) could be susceptible to turbulence-induced reproductive impairment associated with hydrodynamic shear. Further experiments are necessary to test for such potential generality, and to

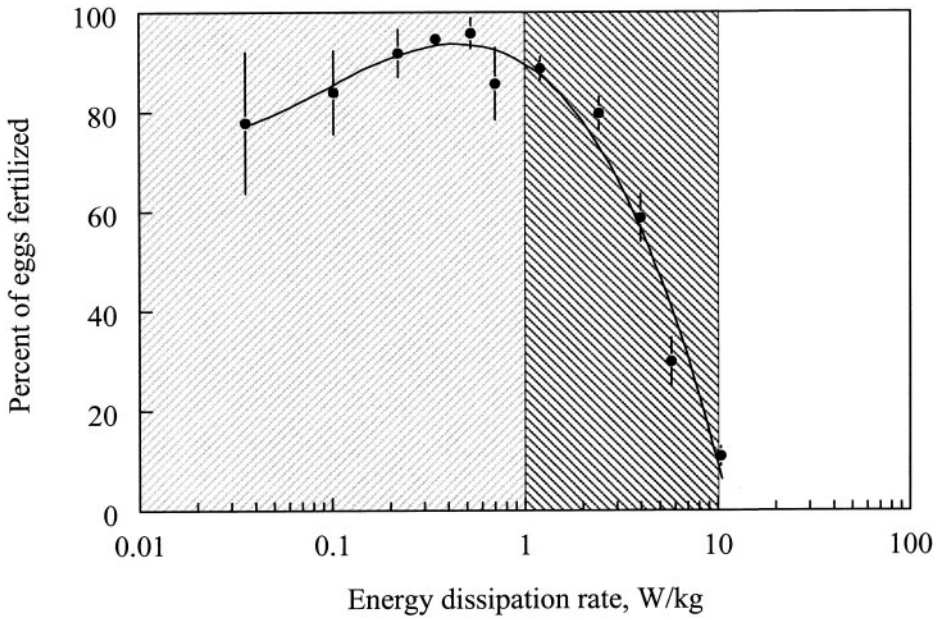

Figure 3. Short-term to long-term average energy dissipation rates recorded in the present study extended into the critical range where prior laboratory experiments with *Strongylocentrotus purpuratus*, the purple sea urchin, showed marked declines in fertilization. Light shading indicates the measured range of long-term average energy dissipation rates; heavy shading indicates the range of energy dissipation rates observed over short durations spanning 0.128 s. Data points and error bars are redrawn from Denny *et al.* (3).

determine whether other known life histories (*e.g.,* release of gametes in viscous mucus [12,13], spawning during large wave events [14]) might alter relationships between species and the environmental turbulence they encounter.

Acknowledgments

I thank two anonymous reviewers who sharpened the presentation. Funding was provided by NSF grants OCE-9313891, OCE-024117, OCE-0523870, and the University of California Marine Council Coastal Environmental Quality Initiative grant 04-T-CEQI-08-0048. Contribution 2410 from the Bodega Marine Laboratory, University of California at Davis.

Literature Cited

1. **Levitan, D. R. 1995.** The ecology of fertilization in free-spawning invertebrates. Pp. 123–156 in *Ecology of Marine Invertebrate Larvae*, L. McEdward, ed. CRC Press, Boca Raton, FL.
2. **Mead, K. S., and M. W. Denny. 1995.** The effects of hydrodynamic shear stress on fertilization and early development of the purple sea urchin *Strongylocentrotus purpuratas*. *Biol. Bull*. **188:** 46–56.
3. **Denny, M. W., E. K. Nelson, and K. S. Mead. 2002.** Revised estimates of the effects of turbulence on fertilization in the purple sea urchin, *Strongylocentrotus purpuratus*. *Biol. Bull*. **203:** 275–277.
4. **Mead, K. S., and D. Epel. 1995.** Beakers *versus* breakers: how fertilisation in the laboratory differs from fertilisation in nature. *Zygote* **3:** 95–99.
5. **Denny, M., J. Dairiki, and S. Distefano. 1992.** Biological consequences of topography on wave-swept rocky shores. I. Enhancement of external fertilization. *Biol. Bull*. **183:** 220–232.
6. **Thornton, E. B., and R. T. Guza. 1983.** Transformation of wave height distribution. *J. Geophys. Res*. **88:** 5925–2938.
7. **Gaylord, B. 1999.** Detailing agents of physical disturbance: wave-induced velocities and accelerations on a rocky shore. *J. Exp. Mar. Biol. Ecol*. **239:** 85–124.
8. **Gaylord, B. 2000.** Biological implications of surf-zone flow complexity. *Limnol. Oceanogr*. **45:** 174–188.
9. **Tennekes, H., and J. L. Lumley. 1972.** *A First Course in Turbulence*. MIT Press, Cambridge, MA.
10. **George, R., R. E. Flick, and R. T. Guza. 1994.** Observations of turbulence in the surf zone. *J. Geophys. Res*. **99:** 801–810.
11. **Baker, M. A., and C. H. Gibson. 1987.** Sampling turbulence in the stratified ocean: statistical consequences of strong intermittency. *J. Phys. Oceanogr*. **17:** 1817–1836.
12. **Yund, P. O., and S. K. Meidel. 2003.** Sea urchin spawning in benthic boundary layers: Are eggs fertilized before advecting away from females? *Limnol. Oceanogr*. **43:** 795–801.
13. **Thomas, F. I. M. 1994.** Physical properties of gametes in three sea urchin species. *J. Exp. Biol.* **194:** 263–284.
14. **Shanks, A. L. 1998.** Apparent oceanographic triggers to the spawning of the limpet *Lottia digitalis* (Rathke). *J. Exp. Mar. Biol. Ecol.* **222:** 31–41.
15. **Svendsen, I. A. 1978.** Analysis of surf zone turbulence. *J. Geophy. Res*. **92:** 5115–5124.